

Compressed Sensing of Scanning Transmission Electron Microscopy (STEM) on

Non-Rectangular Scans

Xin Li^{1,2,3,4}, Ondrej Dyck^{1,2}, Sergei V. Kalinin^{1,2*} and Stephen Jesse^{1,2*}

¹Institute for Functional Imaging of Materials, Oak Ridge National Laboratory, Oak Ridge TN 37831, USA

²Center for Nanophase Materials Sciences, Oak Ridge National Laboratory, Oak Ridge TN 37831, USA

³Department of Industrial Engineering, Florida State University, Tallahassee FL 32306, USA

⁴Department of Statistics, Florida State University, Tallahassee FL 32306, USA

This manuscript has been authored by UT-Battelle, LLC, under Contract No. DE-AC05-00OR22725 with the U.S. Department of Energy. The United States Government retains and the publisher, by accepting the article for publication, acknowledges that the United States Government retains a non-exclusive, paid-up, irrevocable, world-wide license to publish or reproduce the published form of this manuscript, or allow others to do so, for the United States Government purposes. The Department of Energy will provide public access to these results of federally sponsored research in accordance with the DOE Public Access Plan (<http://energy.gov/downloads/doe-public-access-plan>)

Abstract

Scanning Transmission Electron Microscopy (STEM) has become the main stay for materials characterization on atomic level, with applications ranging from visualization of localized and extended defects to mapping order parameter fields. In the last several years, attention was attracted by potential of STEM to explore beam induced chemical processes and especially manipulating atomic motion, enabling atom-by-atom fabrication. These applications, as well as traditional imaging of beam sensitive materials, necessitate increasing dynamic range of STEM between imaging and manipulation modes, and increasing absolute scanning speed, that can be achieved by combining sparse sensing methods with non-rectangular scanning trajectories. Here we developed a general method for real-time reconstruction of sparsely sampled images from high-speed, non-invasive and diverse scanning pathways including spiral scan and Lissajous scan. This approach is demonstrated on both the synthetic data and the experimental STEM data on the beam sensitive material graphene. This work opens the door for comprehensive investigation and optimal design on dose efficient scanning strategies and real-time adaptive inference and control of e-beam induced atomic fabrication.

Keywords

STEM, Compressed Sensing, Image Inpainting, Real-time, Sprial Scan , Lissajous Scan, Non-Rectangular Scan, GPU

Introduction

Scanning transmission electron microscopy (STEM) has emerged as an extremely versatile imaging tool to analyze materials at atomic resolution (S. J. Pennycook 2017): extending from Albert Crewe's initial demonstration of single atom detection (Crewe, Wall, and Langmore 1970) to atomically resolved electron energy loss spectroscopy (EELS) (Browning, Chisholm, and Pennycook 1993; Batson 1993) and the ability of Z-contrast imaging to directly reveal structure and chemistry (Krivanek et al. 2010). The successful implementation of aberration correction not only led to record breaking resolution, (H. Rose 1974; Findlay et al. 2009; Okunishi et al. 2009; Findlay et al. 2010) but also improved contrast and revealed the potential for 3D imaging through depth sectioning enabled by high convergence angles (Albina Y Borisevich, Lupini, and Pennycook 2006; A. Y. Borisevich and Y. 2006; van Benthem et al. 2005, 2006). Another impressive achievement that has been developed in recent years is the ability of EELS to access vibrational spectroscopic signals (Krivanek et al. 2014), adding another feather in an already impressive cap of characterization tools.

The characteristic aspect enabling the EELS modality is the energy transfer from the electron beam to a material sample, including both the electronic and ionic sub-systems (Egerton 2011). One manifestation of this is electron beam damage which can be brought on by direct nuclear recoil (knock-on), beam heating, radiolysis, and induced electric fields (Jiang 2016) and is generally viewed as an effect to be avoided. Indeed, there was some question as to whether successful aberration correction would exacerbate beam damage to such an extent that it would render the advance useless (S. J. Pennycook 2017). Fortunately, it turned out not to be so. Nevertheless, various strategies have been employed to reduce electron dose such as repeated

fast scans(Zhou et al. 2012) and more efficient use of the available electrons(T. J. Pennycook et al. 2015; McMullan et al. 2009, 2014). It seems clear that improvements on this front will manifest in the near future where highly efficient detectors will be coupled with sparse sampling techniques for real-time, low dose imaging.

This issue has become especially acute with the recognition that the e-beam can be used for atomic scale fabrication(Kalinin, Borisevich, and Jesse 2016; Zhao et al. 2017; Kalinin and Pennycook 2017; Jiang et al. 2017; Susi et al. 2014). Recent efforts to manipulate single atoms with the electron beam have established that such capabilities are possible, with the introduction (Dyck et al. 2017), movement (Susi, Meyer, and Kotakoski 2017; Susi et al. 2017) of atoms in a graphene lattice being demonstrated. Such abilities rely on the material or atom in question to be close to being damaged by the beam. Because the same beam is used for imaging and manipulation, one must alternate between manipulation and imaging modalities in attempts to modify and then observe the sample. This requires both increasing the dynamic range of STEM between imaging and manipulation, and increase of imaging speed, as a prerequisite to enable real-time analysis and feedback mechanisms(Jesse et al. 2015, 2018). This will act to decrease the time required for observation as well as decrease the likelihood of unintentional modification of the structure being fabricated.

Recently, the approach for sparse sensing as a pathway for low-dose STEM imaging was broadly introduced by Stevens and Browning(Andrew Stevens et al. 2014; Kovarik et al. 2016; A. Stevens et al. 2018). However, these approaches were implemented invariably for the rectangular scans of the commercial STEM systems, where the scan path is the zig-zag pattern over a rectangular area (raster scan). In other words, the electron beam is scanned from left to

right, then “flies” back to the left side and scans the next row proceeding more slowly from top to bottom. A problem with this type of scan is the so-called fly-back distortion (Muller and Grazul 2001; Jones and Nellist 2013). This occurs due to hysteresis in the scan coils and is typically addressed by applying a delay between the fly-back step and the beginning of the next scan line which allows the scan coils to stabilize. For scanned images acquired over dozens of seconds, this delay may be an acceptably small fraction of the image acquisition time. However, because this delay is the same no matter how quickly the image is acquired, it may pose a significant lower bound on the speed with which acquisition can occur. The alternative scan paths introduced recently offer an improvement for scanning speed (Sang et al. 2017).

Here, we introduce a general method for real-time reconstruction of sparsely sampled images from high-speed, non-invasive and diverse scanning pathways. A critical requirement for the practical application of such a method, assuming reliable reconstruction is given, is that it must be fast enough to operate in real time (magnitudes faster than scanning duration). To ensure its applicability in this regard, it is deployed via an NVIDIA Titan X Pascal graphics processing unit (GPU) to evaluate its performance in a favorable yet realistic context (i.e. having the computational muscle of a supercomputing cluster is certainly possible but employing a local GPU-accelerated process is much more accessible and likely). The source code used for the investigations described has been made available online. This approach is demonstrated on the beam sensitive material graphene, for both the synthetic data and the operating STEM experiments.

Materials and Methods

Real-time Image Inpainting

We want to recover the (unknown) full STEM image, \mathbf{f}_0 , from sparse and noisy measurements \mathbf{y} that can be obtained from various scanning pathways including spiral scan, raster scan, random scan and Lissajous scan that are demonstrated numerically and experimentally in following sections. Besides the noisy measurements, another input is the sampling mask, which indicates the spatial locations from which we have acquired the measurements, and it can be precomputed given scanning pathway and output image size. We express this in mathematical terms as,

$$\mathbf{y} = \mathbf{\Phi}\mathbf{f}_0 + \boldsymbol{\epsilon} \quad (1)$$

where $\boldsymbol{\epsilon}$ is the measurement noise and $\mathbf{\Phi}$ is the masking operator, defined by

$$(\mathbf{\Phi}\mathbf{y})_p \stackrel{\text{def}}{=} \begin{cases} y_p & \text{if } p \in \mathbf{M} \\ 0 & \text{otherwise} \end{cases} \quad (2)$$

where \mathbf{M} is a binary mask indicating pixel locations sampled by scanning pathways.

We focus on using structural sparsity regularization on the redundant wavelet frame (Mallat 2009) to recover an image from the sparse measurements. The reconstructed STEM image $\mathbf{f} = \mathbf{W}\mathbf{x}$ is estimated by optimizing the coefficients \mathbf{x} in the wavelet basis, where \mathbf{W} is the wavelet synthesis operator. To achieve this, we solve the L_1 sparsity regularized image inpainting problem via the iterative thresholding algorithm:(Daubechies, Defrise, and De Mol 2004)

$$\operatorname{argmin}_{\mathbf{x}} = \frac{1}{2} \|\mathbf{y} - \mathbf{\Phi}\mathbf{W}\mathbf{x}\|^2 + \lambda \|\mathbf{x}\|_1 \quad (3)$$

where λ is the tuning parameter controlling the sparsity. The soft thresholding operator plays a key role in the L_1 minimization that shrinks the value of coefficients:

$$S_\lambda(x) = x * \max(0, 1 - \frac{\lambda}{|x|}) \quad (4)$$

We denote the soft thresholding operator in wavelet basis as:

$$S_{\lambda}^W(\mathbf{f}) = \sum_m S_{\lambda}(\langle \mathbf{f}, \mathbf{w}_m \rangle) \mathbf{w}_m \quad (5)$$

where \mathbf{w}_m is the basis of the wavelet frame $\mathbf{W} = \{\mathbf{w}_m\}$. Specifically, we focus on the Daubechies wavelets (Daubechies 1992), a family of orthogonal wavelets.

Following derivations in the iterative thresholding algorithm (Daubechies, Defrise, and De Mol 2004; Peyré 2011), each iteration computes:

$$\mathbf{f}^{(i+1)} = S_{\lambda}^W(\text{ProjC}(\mathbf{f}^{(i)})) \quad (6)$$

where $\text{ProjC}(\mathbf{f})$ computes the gradient descent of the data fidelity term $\frac{1}{2} \|\mathbf{y} - \Phi \mathbf{W} \mathbf{x}\|^2$:

$$\text{ProjC}(\mathbf{f}) = \mathbf{M} \mathbf{y} + (1 - \mathbf{M}) \mathbf{f} \quad (7)$$

To get real-time image inpainting from sparse scan measurements that is instrumental for future tasks such as real-time in-situ atom motion tracking, we developed a parallel implementation for the above iterative thresholding algorithm utilizing the CUDA toolkit of the NVIDIA Corporation. It costs around 0.008 seconds to reconstruct a STEM image (synthetic and experimental) of size 256 by 256.

Sparse Spiral Scan

We design a field-programmable gate array (FPGA)-based scan system (built upon a National Instruments PXIe-1073 chassis) capable of interfacing with various microscopes. A LabView routine is developed to generate voltage waveforms with input coordinates from customized Matlab code, enabling arbitrary and dynamic beam positioning.

Although the real-time image inpainting algorithm is adapted to various scanning pathways as demonstrated in later sections, we begin by consideration of the special shape of an Archimedean spiral that avoids abrupt changes in scanning direction and has less requirements on beam control hardware, making it an efficient and hardware-friendly scanning strategy

practically. Additional discussion regarding spiral scans and the associated advantages over raster scans can be found at (Sang et al. 2017). One can directly control the total scanning duration as well as electron distribution sparseness via Archimedean spiral scan whose scanning pathway is determined by Eq. (8):

$$\mathbf{x} = A\mathbf{T} \cos(\omega\mathbf{T}), \mathbf{y} = A\mathbf{T} \sin(\omega\mathbf{T}) \quad (8)$$

Given the fixed hardware data IO_rate (the rate of reading data from microscope to computer memory) r , the sampling time sequence \mathbf{T} is determined by the total scanning duration D , $\mathbf{T} = [0, D]$ with a step size of $\frac{1}{r}$. In practice, we normalize the \mathbf{T} to $[0,1]$ with the step size of $\frac{1}{rD}$. In this way, one can control the physical scanning area directly by the amplitude parameter, A . Taking the derivative of Eq. (8), at a particular sampling time point, t , we get the scanning beam velocity with a magnitude:

$$|\vec{v}| = A\sqrt{1 + \omega^2 t^2} \approx A\omega t \quad (9)$$

and the magnitude of angular velocity is defined by:

$$\Omega = \frac{|\vec{v}|}{r} = \frac{A\omega t}{t} = A\omega \quad (10)$$

As the sampling time increases, the spiral is drawn outward beginning at the origin with the increasing velocity magnitude. This means that the center of the spiral will be more densely sampled than the outer edge. Meanwhile, given the total scanning duration, smaller frequency ω (angular velocity) will result in a shorter total scan distance, yielding spatial sparseness of electron dose distribution, and will increase the average sampling density (this will improve the

signal-to-noise ratio in practice), improving evenness of electron dose distribution. Figure 1 clearly highlight sparseness and evenness introduced by decreasing frequency ω , where we scatter points on an Archimedean spiral with $\omega = 128, 16,$ and 8 (Hz) respectively.

Results

We performed all the experiments on the beam sensitive material graphene. CVD-grown graphene samples were transferred from Cu foil to TEM grids and cleaned via a wet transfer method and baking in an ArO₂ environment as described elsewhere (Dyck et al. 2018). The dopant atom was inserted *in situ* as described elsewhere (Dyck et al. 2017). The accelerating voltage was set to be 60 kV for all the HAADF scans in this paper.

The real-time inpainting algorithm only requires the sparse and noisy measurements \mathbf{y} together with the sampling mask \mathbf{M} that can be precomputed offline. Inpainting algorithm has three primary tuning parameters: total iteration number, thresholding value and the level of wavelet. For all the synthetic and experimental datasets, we fixed total iteration number at 10, the thresholding value at 2.4. For scans with amplitude A of 5 (v), we choose the wavelet level to be 2. For less scanning area with the smaller amplitude A of 1 (v), we set the level to be 3, since the atom spans more pixels than those scanned at $A = 5$ (v). We note that reconstruction results can be further improved by fine-tuning of these parameters. To ascertain the performance of the algorithm, we first performed reconstructions with artificially sampled data with Archimedean scan. We use peak-to-signal-noise ratio (PSNR) and the structural similarity index (SSIM (Wang et al. 2004)) for measuring inpainting quality. SSIM returns value of 1 for synthetic ground-truth image compared with itself. All experiments were performed on square images of width $N = 256$.

Synthetic Spiral Scan

Figure 2a is the synthetic ground-truth STEM image for graphene with a single 4-fold silicon dopant without any noise, whose pixel intensities were normalized to [0,1]. We added white Gaussian noise with variance $\delta^2 = 0.80$ to the Archimedean spiral scan path imposed on the ground-truth image. For Archimedean spiral, we set frequency $\omega = 8, 16, 32, 64, 128$ (Hz) with different scanning durations: 0.1, 0.2, 0.4, 0.8, 1.6 (seconds). We fixed IO_rate r at 2000000 Hz and the amplitude A at 1(v). Figure 2b are the sparse and noisy images sampled by Archimedean spiral scans on the ground-truth image. In Figure 2b, we can see the outer region has more noise (a large view in Figure 2d) although the noise variance is fixed along the Archimedean spiral scans. This is because scanning beam moves faster at outer edges, yielding less samples within per pixel location. Figure 2c shows the impressive reconstruction images based on sparse and noisy ones.

Figure 3 and Figure 4 display the SSIM and PSNR values for all sparse and noisy measurements and the corresponding reconstruction results. Interestingly, at shortest scanning duration of 0.1 seconds, reconstruction yielded higher SSIM and PSNR values with smaller frequencies for $\omega = 32, 64, 128$ (Hz). This may be caused by higher average sampling density resulted from smaller frequency as illustrated in Figure 1.

In Figure 5, we also tested the inpainting algorithm results on the standard Lena image for a range of sparseness induced on spiral scans. We can see that the inpainting algorithm could also yield impressive results on the standard image for a general visual inspection purpose, especially for sparsely scanned images with lower frequencies $\omega=8, 16$ Hz. Figure 6 are PSNR and SSIM values for reconstructions on the Lena image.

Experimental Spiral Scan

We first set the amplitude of Archimedean spiral scan at $A = 5$ (v), with $\omega = 16, 32, 64, 128$ (Hz) and durations of 0.1, 0.2, 0.4, 0.8, 1.6, 3.2 (seconds). Figure 7a displays the raw STEM images by Archimedean spiral scans and Figure 7b shows the corresponding inpainted results. Figure 7c is the large view of raw Archimedean spiral scanned image with maxim duration of 6.4 seconds and maxim frequency considered at $\omega = 256$ Hz. Figure 7d,e are the large views of raw and inpainted images from Archimedean spiral scan with duration of 3.2 seconds and $\omega = 32$ Hz. At amplitude voltage of 5 (v), we see the reconstruction could not yield recognizable lattice structure with ω less than 16 Hz. Also, for scans finished less than 0.8 seconds, both raw and inpainted images were severely affected by noise, making it hard to see the atomic structure.

To increase temporal resolution as well as spatial sparseness, we can straightforwardly decrease physical scanning area by reducing the amplitude of Archimedean spiral scan to $A = 1$ (v). For this smaller scanning area, we considered $\omega = 8, 16, 32, 64, 128$ Hz and durations of 0.1, 0.2, 0.4, 0.8, 1.6 seconds. Figure 8a displays raw STEM images by Archimedean spiral scans and Figure 8b shows the corresponding inpainted results. Figure 8c,d are the large views of raw and inpainted images from Archimedean spiral scan with duration of 0.8 seconds and $\omega = 32$ Hz. We note that scan only took 0.8 seconds on the beam sensitive material graphene, meanwhile reliable reconstruction took around 0.008 seconds.

Diverse Scanning Pathways

Besides spiral scan, the Lissajous scan is another promising scanning strategy towards video-rate, high-quality scanning imaging, whose scan trajectory is generally defined as:

$$\mathbf{x} = A_x \cos(2\pi f_x \mathbf{T}), \mathbf{y} = A_y \cos(2\pi f_y \mathbf{T}) \quad (11)$$

where A_x, A_y, f_x, f_y represent the amplitudes and frequencies associated with x, y axes. Previous work (Tuma et al. 2012, 2013; Bazaei, Yong, and Moheimani 2012; Yong et al. 2012) detailed the Lissajous scan properties. Here we demonstrate that the scanning duration and hardware burden can be further reduced by utilizing compressive sensing real-time inpainting algorithm.

We would like to minimize the total scanning duration with low-range frequencies, meanwhile maintain the necessary scanning denseness where acceptable image recovery can be achieved. For Lissajous scan with a finite period T_s , the ratio of f_x, f_y has been proved (Tuma et al. 2013; Bazaei, Yong, and Moheimani 2012) to be a rational number:

$$\frac{f_x}{f_y} = \frac{2N}{2N-1} \quad (12)$$

where N is a positive integer and the period $T_s = \frac{1}{f_x - f_y}$. Without loss of generality, we fix f_x given the scanner mechanical limitations and rewrite the period:

$$T_s = \frac{1}{f_x - f_y} = \frac{1}{f_x - \frac{2N-1}{2N}f_x} = \frac{2N}{f_x} \quad (13)$$

For spatial resolution of Lissajous scan, Bazaei et al. 2012 and Tuma et al. 2013 reported the lowest resolution zone is at the scanned area center. Following the derivation in Bazaei et al 2013, the spatial sparseness of Lissajous scan h , defined as the altitude length of the diamond formed by the four crossing points around the image center, can be approximately calculated via:

$$h \approx \frac{\pi A_x A_y}{N \sqrt{A_x^2 + A_y^2}} \quad (14)$$

Based on Equation (13) and (14), we can see there is a compromise between the spatial sparseness and scanning period. Spatial sparseness can be reduced by increasing N . This will increase the likelihood for a successful inpainting recovery. Meanwhile, scan period is proportional to N . A unique property of Lissajous scan is the multiresolution (Tuma et al. 2012, 2013; Bazaei, Yong, and Moheimani 2012): the resolution of Lissajous scan increase dramatically during the first half of the scan period then tends to be stable, increasing slowly until the end of period. In practice, we propose a general rule for selecting Lissajous scan parameters aided by compressive sensing:

1. Given the hardware limitations, fix the maximum frequency f_x .
2. Find the minimum N that yields acceptable image inpainting results.
3. Perform the scan only during $[0: T_s/2]$ period, instead of the whole period.

Figure 9 shows reconstruction results for Lissajous scans with different N . Here we set $A_x = A_y = 1$, $f_x = 32$ Hz. We consider 4 different scanning periods $T_s = 2.0, 1.6, 1.2, 0.8$ seconds. The actual scanning duration was set to be $\frac{T_s}{2}$ (1.0, 0.8, 0.6, 0.4 seconds). Based on equation (13), we have $N = T_s * f_x / 2 = 32, 26, 19, 13$ (rounded to integer). And f_y can be calculated by equation (12). In Figure 9, we can see that the inpainting algorithm starts to fail when N is decreased to 13. Figure 10 are the corresponding PSNR and SSIM values.

To further demonstrate the broad capability of real-time image inpainting algorithm, Figure 11 shows experimental raster scans and inpainting results. For experimental raster scans, we apply a constant voltage on one scanning direction while another direction is driven by a sine wave. We set duration to be 1.6 seconds with $\omega = 128, 64, 32, 16, 8$ (Hz).

We also considered the random scans on the synthetic ground-truth image. Define the scanning ratio, sr , as the number of scanned pixels over the number of total pixels. We added the white Gaussian noises with $\delta^2 = 0.02, 0.05, 0.10$ and we set $sr = 0.1, 0.2, 0.3, 0.4, 0.5, 0.6, 0.7, 0.8, 0.9$. Figure 12a,b display the sparse and reconstructed images under various sparseness and noise levels. Figure 12c,d are the corresponding SSIM and PSNR values.

Discussion

Recently, (Reed, Park, and Masiel 2016) reported that denoising alone may work well for fully sampled low-dose imaging. Figure 13a is a regularly scanned low-dose HAADF image over a graphene sample. The image is of 256 by 256 pixel size with a pixel dwell time of 16 μ s. The acquisition time was no less than 1 sec ($256*256*16*1e^{-6}$). Accelerating voltage was 60 kV, same with all the other scans in the paper. For the fully scanned low-dose image such as Figure 13a, our inpainting algorithm automatically reduced to the standard wavelet denoising algorithm (for fully sampled images, scanning mask $\mathbf{M}=\mathbf{1}$). Figure 13b is the denoising result by our inpainting algorithm. Figure 13c is the adaptive filter denoising result (MATLAB *wiener2* function with neighborhood of size [15,15]) and Figure 13d is the median filter denoising result (MATLAB *medfilt2* function with neighborhood of size [15,15]). For sparsely sampled images (low-frequency scan) such as Figure 8c, the “denoising only” methods may not yield acceptable reconstructions.

On reducing the scanning duration, a misconception for random sub-sampling is that the total acquisition time can be proportionally reduced by reducing number of sampled pixels (assuming the pixel dwell time fixed). However, it also takes time for the beam to move between sampled pixels. In fact, finding the shortest path connecting randomly located sampling pixels is

a NP-hard problem (the travelling salesman problem). Here we explore multiple hardware-friendly scan pathways with smooth and continuous input voltages, trying to reduce beam movement distance/time to cover the scanned area, at the cost of sparseness that may be relieved by inpainting algorithm.

We provided a variety of scanning settings to show the limits for the inpainting algorithm. Both the sparseness and unevenness in the sampling density will affect the success of reconstruction. For successful reconstructions, neither the frequency nor duration can be too low. For high degree of sparseness as in Fig 11k, the inpainted image shows more of the scan pattern than the sample. Increasing frequency does not necessarily reduce the negative effects on reconstruction made by decreasing the duration. For example, in Figure 8, we can see the reconstruction under $w=128$ Hz, $D=0.1$ sec is worse than that under $w=16$ Hz, $D=1.6$ sec. Future work could be the establishment of a rigorous and systematic mathematical optimization framework for finding “optimal” scanning pathways accounting for hardware constraints as well as sparseness distribution where inpainting algorithm works. For example, the inner region of spiral scan is more densely sampled, on the contrary, the outer area of Lissajous scan is more densely sampled. A “optimal” scanning pathway may be designed to combine advantages of spiral and Lissajous scans, with a more uniformly distributed sampling density (dose rate).

In the foreseeable future, the very same e-beam is used for both imaging mode and fabrication mode. With little hardware updates and cost, our work increases the imaging temporal resolution, enabling the real-time imaging feedback mechanism. One immediate follow-up is incorporating current setting into live data stream from microscope to perform imaging-driven, adaptive inference of e-beam induced dynamical systems, utilizing recently

developed statistical learning approaches. Another uptake for the STEM community is that our work opens the door for the comprehensive investigation and optimal design on dose efficient scanning strategies. To further stimulate the progress for STEM community, we open source the code online.

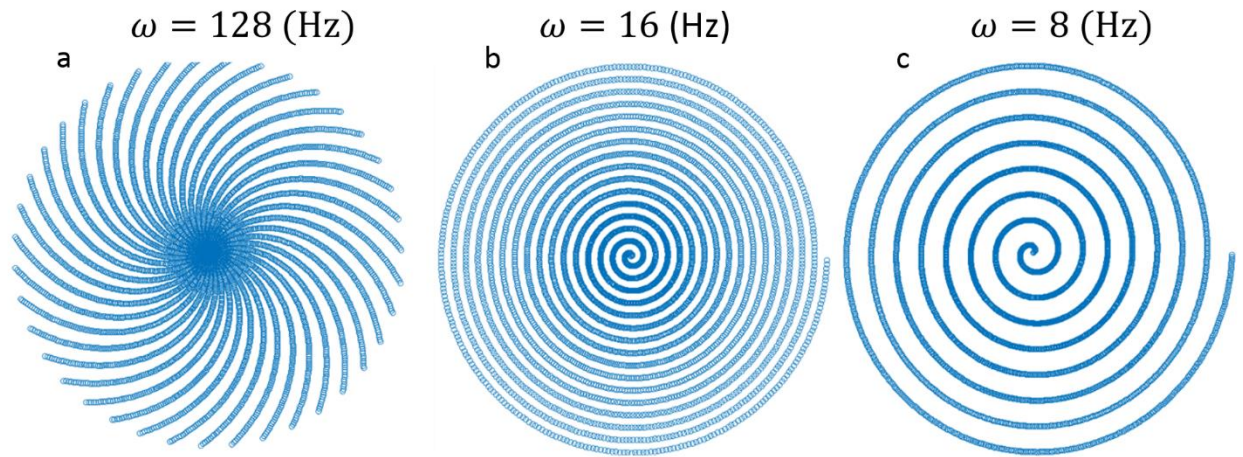


Figure 1: Dose distribution sparseness and evenness induced by small ω on Archimedean spiral scan trajectory: Scatter plots of (x,y) coordinates in scan trajectories with scanning frequencies (a) $\omega = 128$ (Hz), (b) $\omega = 16$ (Hz) and (c) $\omega = 8$ (Hz). For all the three scanning frequencies, we fixed IO_rate $r = 200000$ Hz, total scanning duration $D = 0.05$ seconds and amplitude $A = 1$ v.

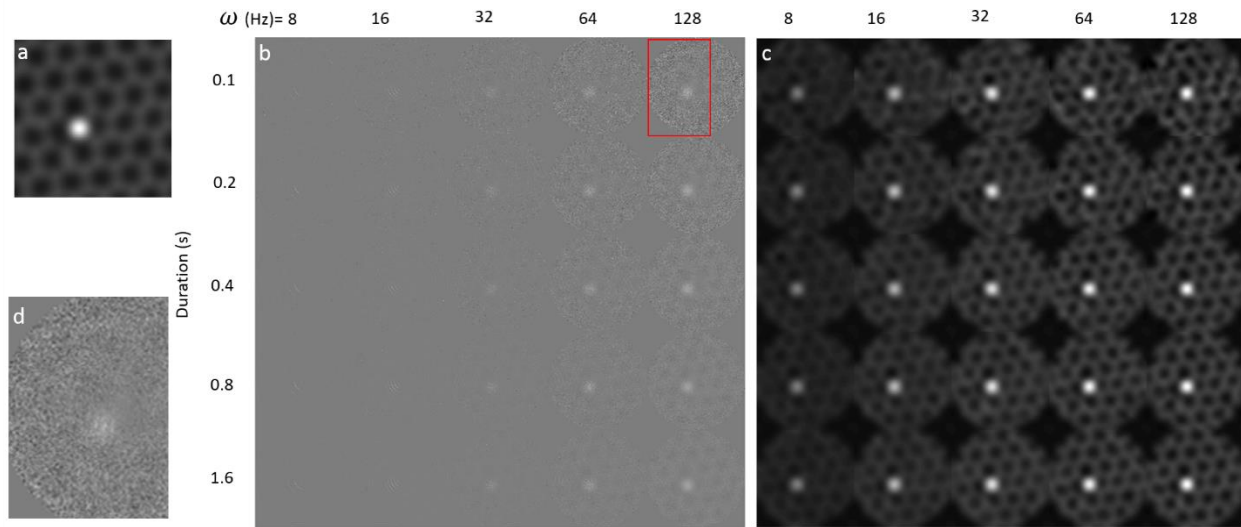


Figure 2: Synthetic Spiral Scan. (a) Ground-truth image. (b) Sparse and noisy Archimedean spiral scans over the ground-truth image. (c) Reconstructed images. (d) A larger view inside the marker in (b).

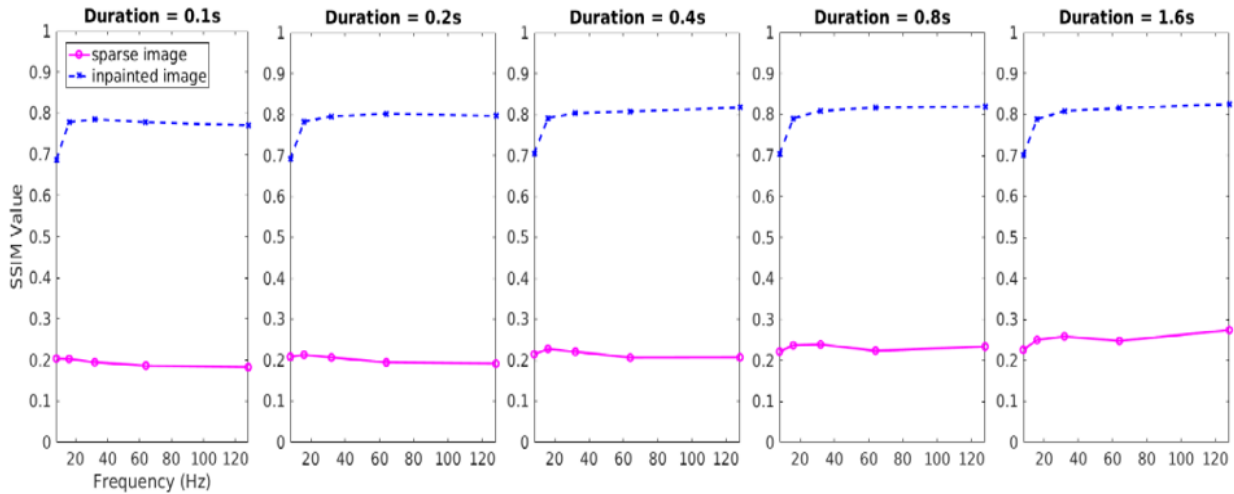


Figure 3: SSIM values of sparse and reconstruction images on synthetic spiral scans.

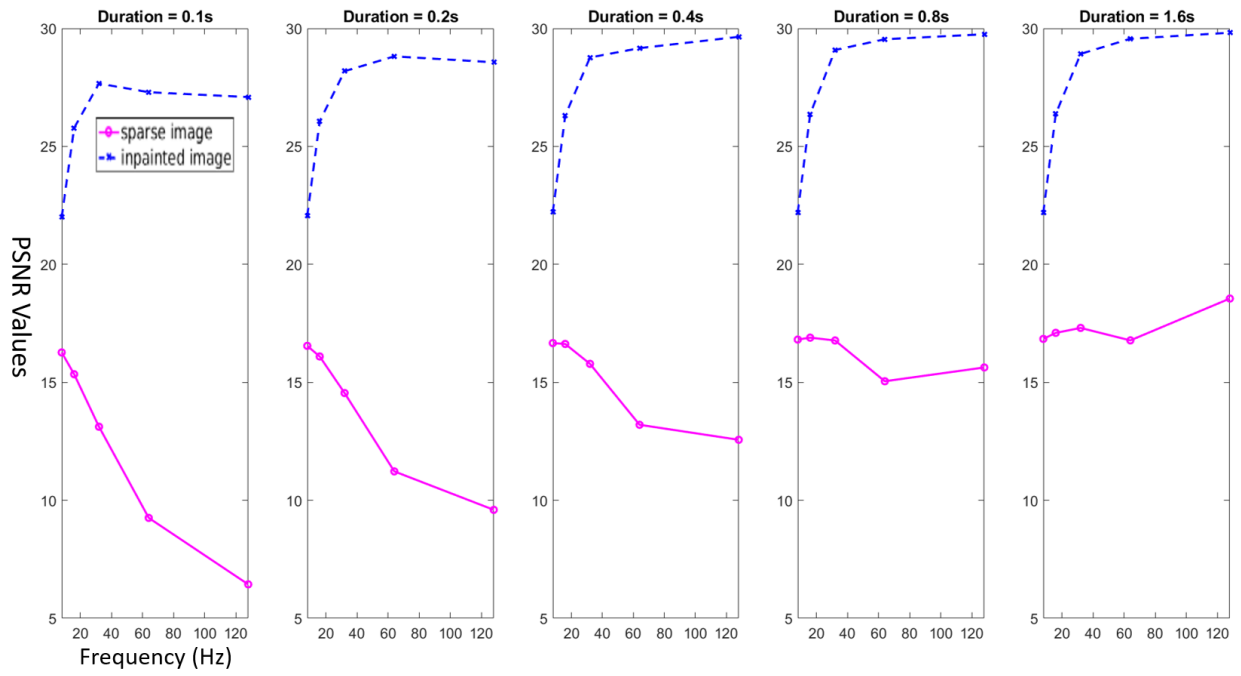


Figure 4: PSNR values of sparse and reconstruction images on synthetic spiral scans.

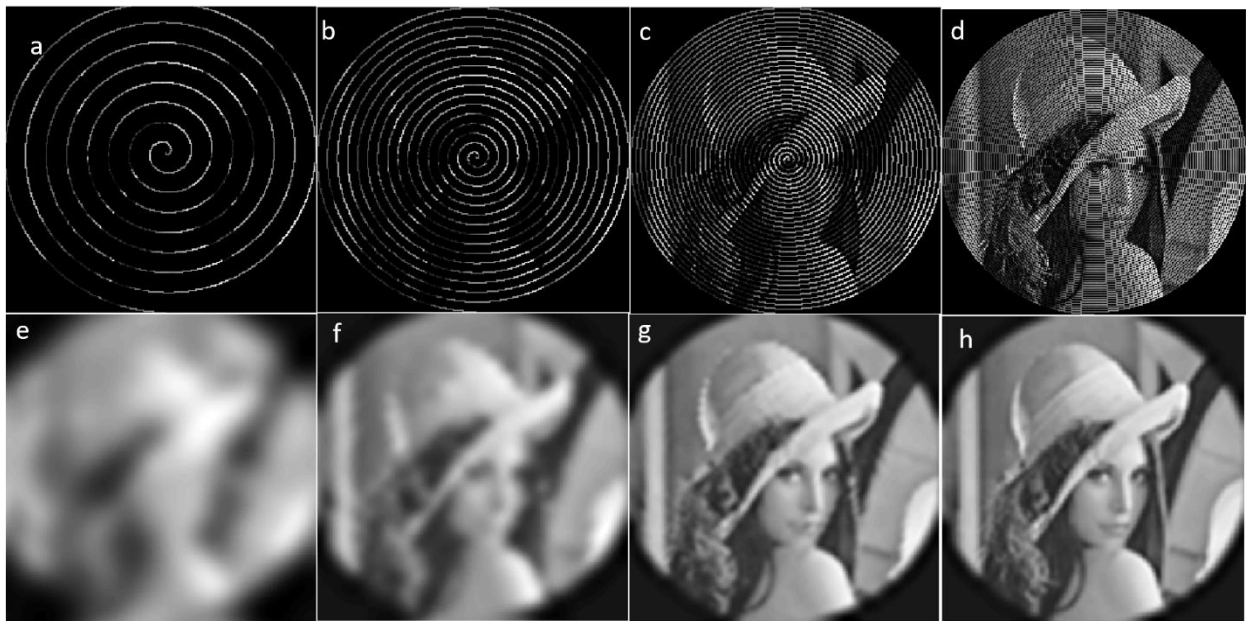


Figure 5: Sparse spiral scans and reconstructions on the Lena image.

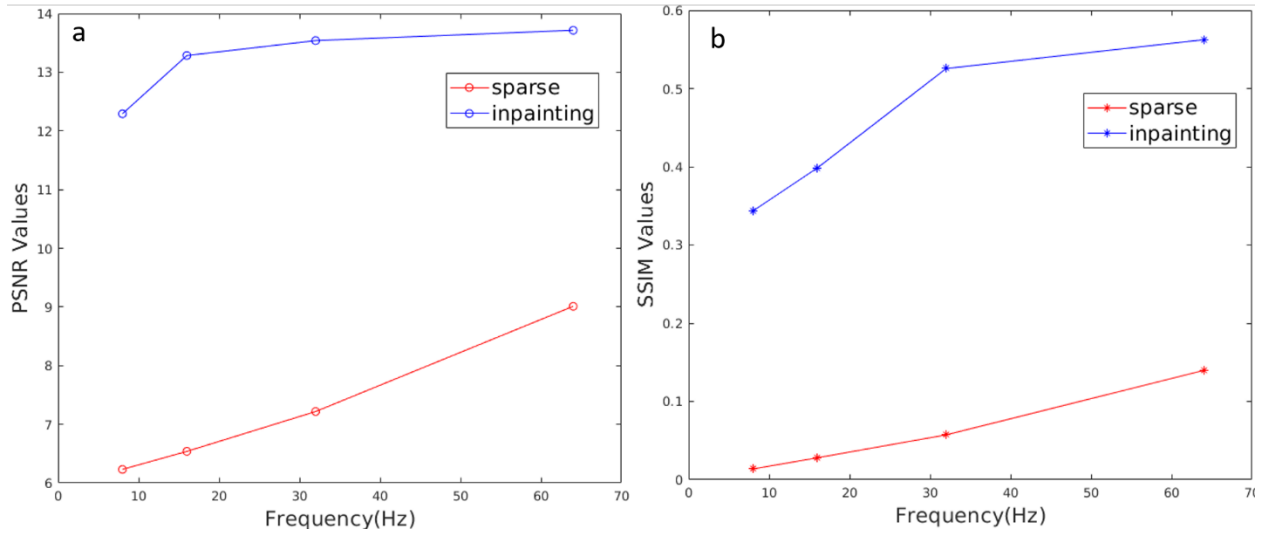


Figure 6: PSNR and SSIM values sparse spiral scans and reconstruction images on the Lena image.

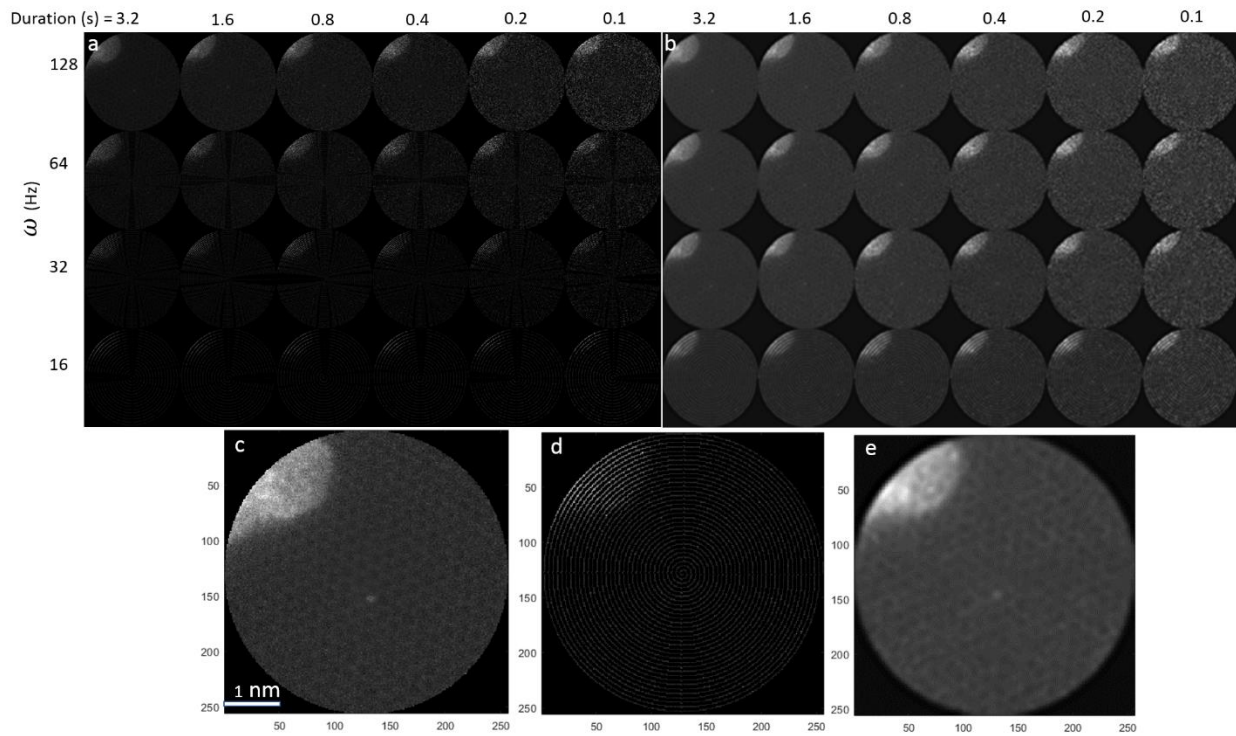


Figure 7: Experimental Archimedean spiral scans with voltage of $A = 5$ (v). (a,b) Raw and inpainted images. (c) Raw STEM image from Archimedean spiral scan with duration of 6.4

seconds and frequency of 256 Hz. (d,e) Large views of raw and inpainted images from Archimedean spiral scan with duration of 3.2 seconds and frequency of 32 Hz.

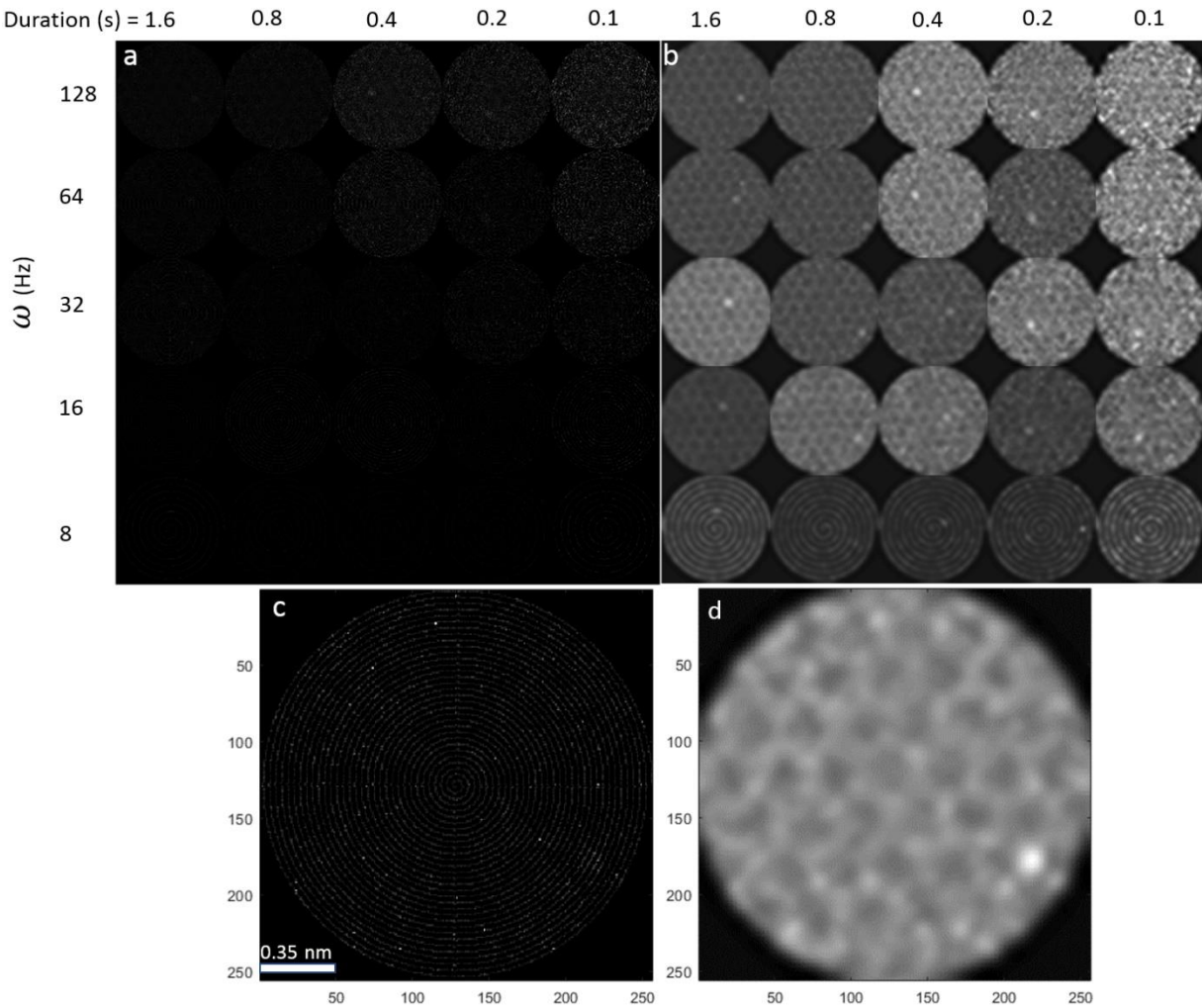


Figure 8: Experimental Archimedean spiral scans with voltage of $A = 1$ (v). (a,b) Raw and inpainted images. (c,d) Large views of raw and inpainted images from Archimedean spiral scan with duration of 0.8 seconds and frequency of 32 Hz.

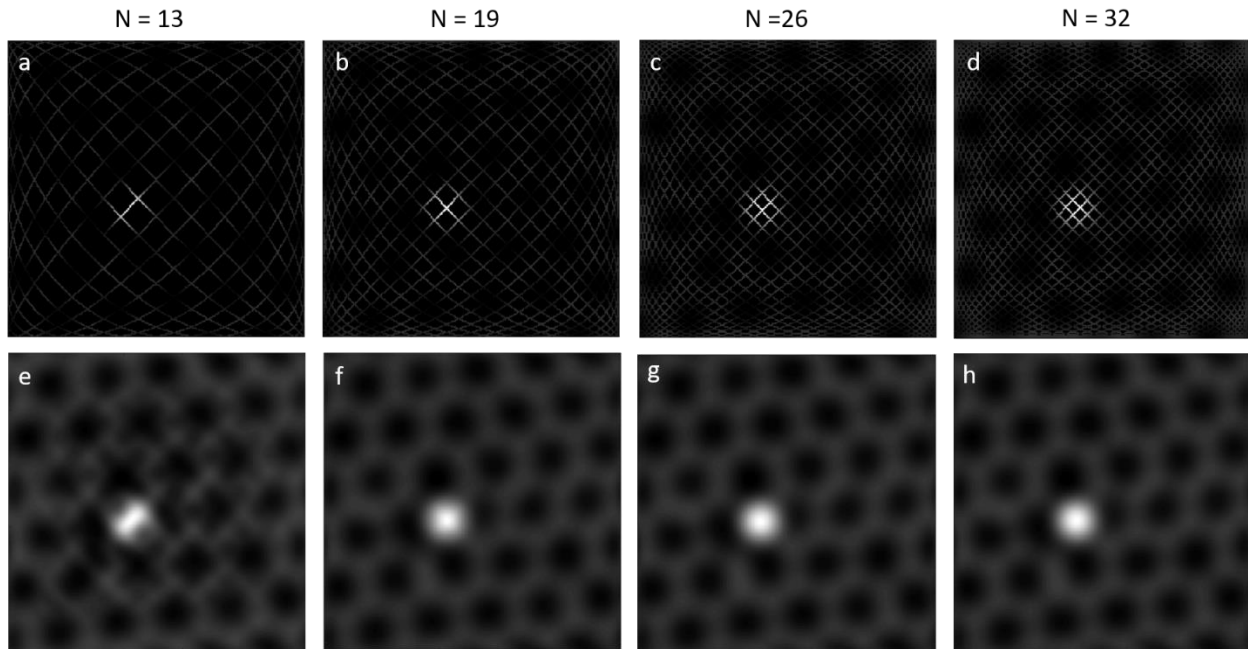


Figure 9: Synthetic Lissajous scans. (a-d) Sparse and noisy images. (e-h) Corresponding inpainting results.

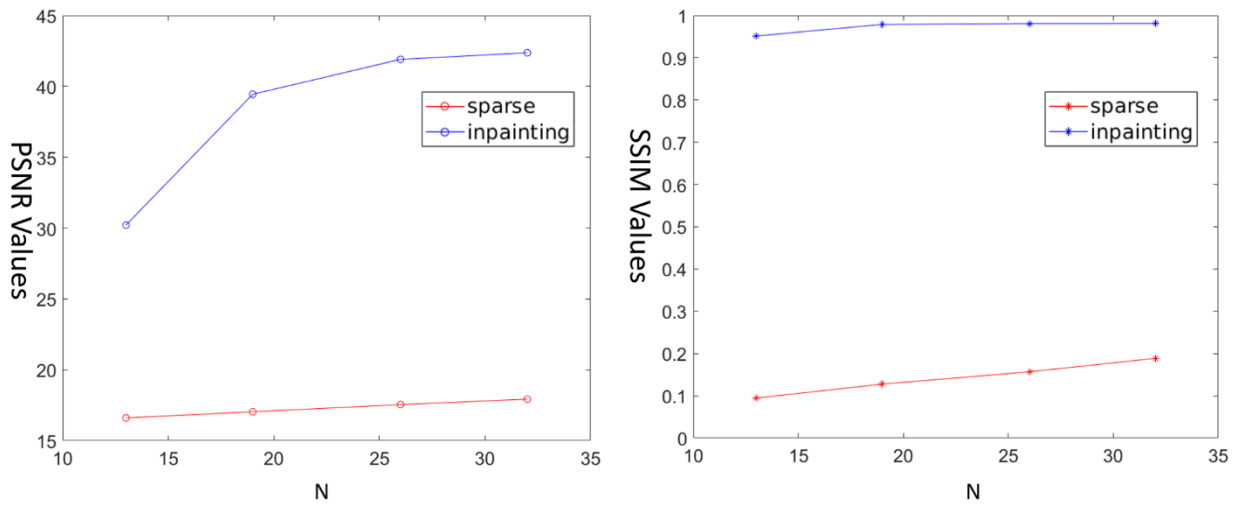


Figure 10: PSNR and SSIM values of sparse and reconstruction images on synthetic Lissajous scans.

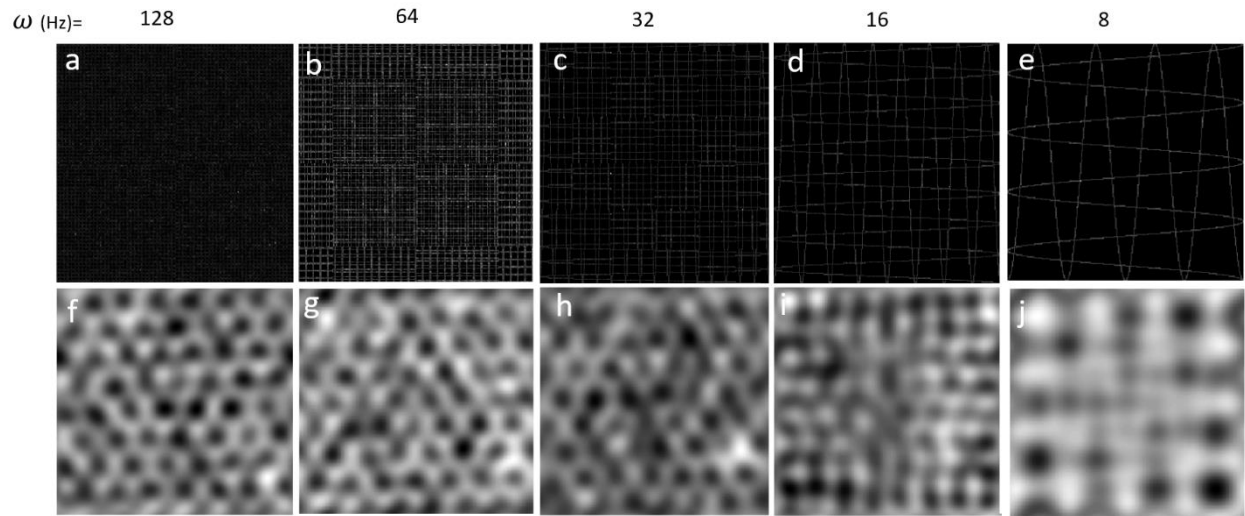


Figure11: Experimental raster scans. (a-e) Sparse and noisy images. (f-j) Corresponding inpainting results.

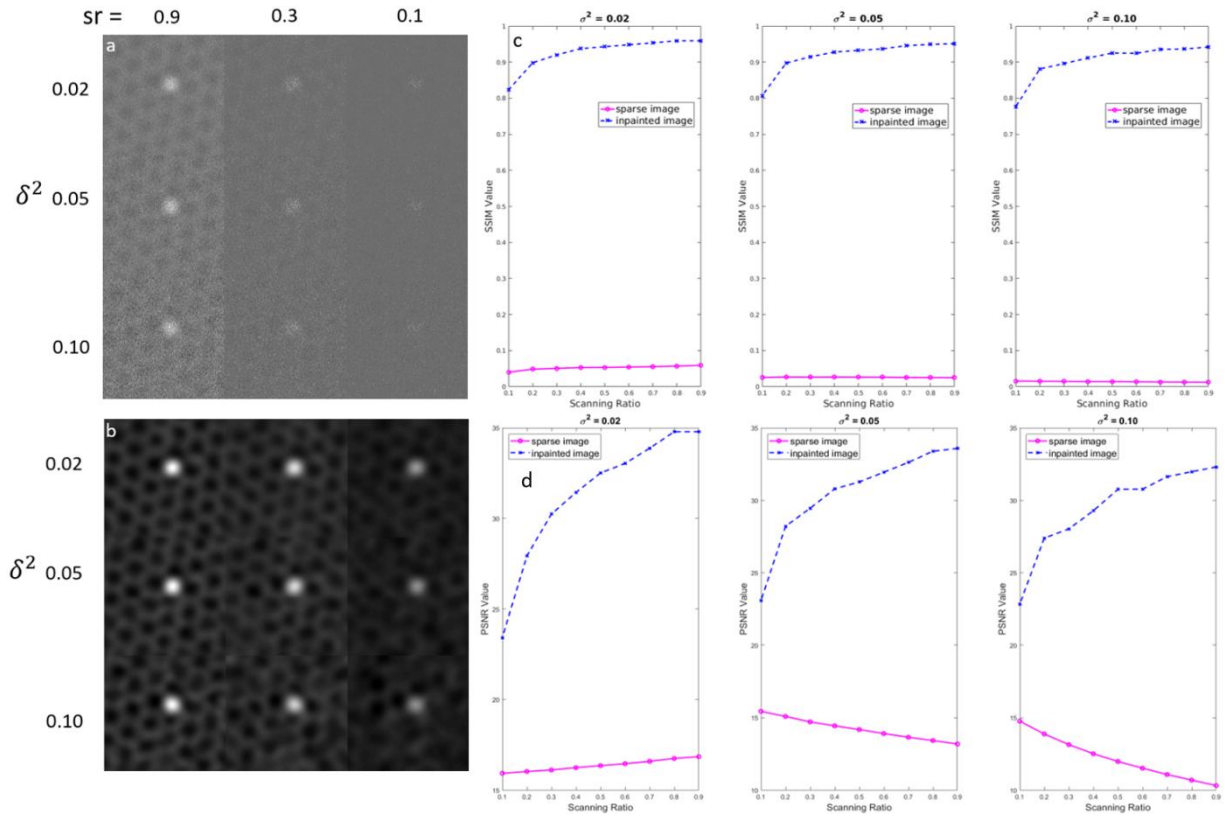


Figure12: Synthetic random scans. (a) Sparse and noisy images. (b) Inpainted results. (c,d)

Numerical evaluations by SSIM and PSNR.

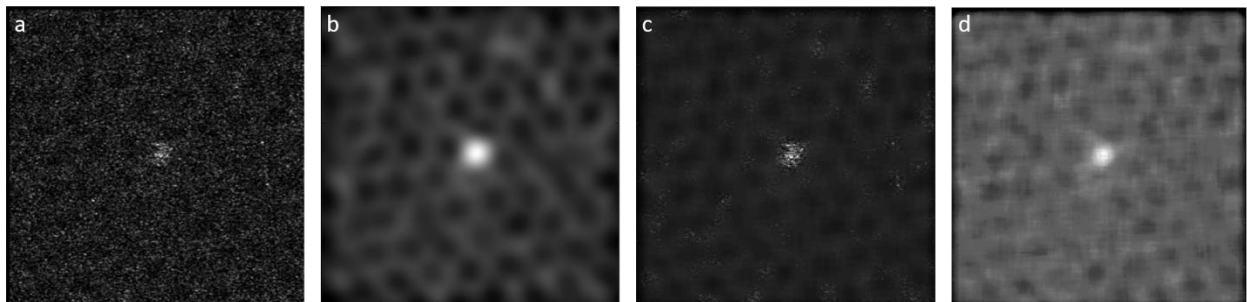


Figure 13: (a) A regularly scanned low-dose HAADF image over a graphene sample. The image is of 256 by 256 pixel size with a pixel dwell time of 16 us. The accelerating voltage is 60 kV. (b) Denoising results by the proposed inpainting algorithm. (c) Denoising result by the adaptive filtering. (d) Denoising result by the median filter.

Data Availability

The data that support the findings of this study are available from the corresponding authors upon request. The source code can be found at <https://github.com/nonmin/RTSSTEM>. The wavelet transform is based on the PDWT(Paleo 2016) package.

Acknowledgements

This research was conducted at the Center for Nanophase Materials Sciences, which is a DOE Office of Science User Facility. S.V.K and S.J. acknowledges the DOE FWP program. We gratefully acknowledge the support of NVIDIA Corporation with the donation of the Titan X Pascal GPU used for this research.

References

- Batson, P. E. 1993. "Simultaneous STEM Imaging and Electron Energy-Loss Spectroscopy with Atomic-Column Sensitivity." *Nature* 366 (6457): 727–28.
<https://doi.org/10.1038/366727a0>.
- Bazaei, A., Yuen K. Yong, and S. O. Reza Moheimani. 2012. "High-Speed Lissajous-Scan Atomic Force Microscopy: Scan Pattern Planning and Control Design Issues." *Review of Scientific Instruments* 83 (6): 063701. <https://doi.org/10.1063/1.4725525>.
- Bentham, Klaus van, Andrew R. Lupini, Miyoung Kim, Hion Suck Baik, SeokJoo Doh, Jong-Ho Lee, Mark P. Oxley, et al. 2005. "Three-Dimensional Imaging of Individual Hafnium Atoms inside a Semiconductor Device." *Applied Physics Letters* 87 (3): 034104.
<https://doi.org/10.1063/1.1991989>.
- Bentham, Klaus van, Andrew R. Lupini, Mark P. Oxley, Scott D. Findlay, Leslie J. Allen, and Stephen J. Pennycook. 2006. "Three-Dimensional ADF Imaging of Individual Atoms by through-Focal Series Scanning Transmission Electron Microscopy." *Ultramicroscopy* 106 (11–12): 1062–68. <https://doi.org/10.1016/J.ULTRAMIC.2006.04.020>.
- Borisevich, A. Y., and A. Y. 2006. "Depth Sectioning of Aligned Crystals with the Aberration-Corrected Scanning Transmission Electron Microscope." *Journal of Electron Microscopy* 55 (1): 7–12. <https://doi.org/10.1093/jmicro/dfi075>.
- Borisevich, Albina Y, Andrew R Lupini, and Stephen J Pennycook. 2006. "Depth Sectioning with the Aberration-Corrected Scanning Transmission Electron Microscope." *Proceedings of the National Academy of Sciences of the United States of America* 103 (9): 3044–48.

<https://doi.org/10.1073/pnas.0507105103>.

Browning, N. D., M. F. Chisholm, and S. J. Pennycook. 1993. "Atomic-Resolution Chemical Analysis Using a Scanning Transmission Electron Microscope." *Nature* 366 (6451): 143–46. <https://doi.org/10.1038/366143a0>.

Crewe, A V, J Wall, and J Langmore. 1970. "Visibility of Single Atoms." *Science (New York, N.Y.)* 168 (3937): 1338–40. <https://doi.org/10.1126/science.168.3937.1338>.

Daubechies, Ingrid. 1992. *Ten Lectures on Wavelets*. siam.

Daubechies, Ingrid, Michel Defrise, and Christine De Mol. 2004. "An Iterative Thresholding Algorithm for Linear Inverse Problems with a Sparsity Constraint." *Communications on Pure and Applied Mathematics*. <https://doi.org/10.1002/cpa.20042>.

Dyck, Ondrej, Songkil Kim, Sergei V. Kalinin, and Stephen Jesse. 2017. "Placing Single Atoms in Graphene with a Scanning Transmission Electron Microscope." *Applied Physics Letters*. <https://doi.org/10.1063/1.4998599>.

———. 2018. "E-Beam Manipulation of Si Atoms on Graphene Edges with Aberration-Corrected STEM." *Journal of Vacuum Science & Technology B*, January. <http://arxiv.org/abs/1710.10338>.

Egerton, R.F. 2011. *Electron Energy-Loss Spectroscopy in the Electron Microscope*. Springer US. https://doi.org/10.1007/978-1-4419-9583-4_2.

Findlay, S. D., N. Shibata, H. Sawada, E. Okunishi, Y. Kondo, T. Yamamoto, and Y. Ikuhara. 2009. "Robust Atomic Resolution Imaging of Light Elements Using Scanning Transmission

Electron Microscopy." *Applied Physics Letters* 95 (19): 191913.

<https://doi.org/10.1063/1.3265946>.

Findlay, S D, N Shibata, H Sawada, E Okunishi, Y Kondo, and Y Ikuhara. 2010. "Dynamics of Annular Bright Field Imaging in Scanning Transmission Electron Microscopy." *Ultramicroscopy* 110 (7): 903–23. <https://doi.org/10.1016/j.ultramic.2010.04.004>.

H. Rose. 1974. "PHASE CONTRAST IN SCANNING TRANSMISSION ELECTRON MICROSCOPY." *OPTIK* 39: 416–36.

Jesse, Stephen, Qian He, Andrew R. Lupini, Donovan N. Leonard, Mark P. Oxley, Oleg Ovchinnikov, Raymond R. Unocic, et al. 2015. "Atomic-Level Sculpting of Crystalline Oxides: Toward Bulk Nanofabrication with Single Atomic Plane Precision." *Small* 11 (44): 5895–5900. <https://doi.org/10.1002/sml.201502048>.

Jesse, Stephen, Bethany M Hudak, Eva Zarkadoula, Jiaming Song, Artem Maksov, Miguel Fuentes-Cabrera, Panchapakesan Ganesh, et al. 2018. "Direct Atomic Fabrication and Dopant Positioning in Si Using Electron Beams with Active Real-Time Image-Based Feedback." *Nanotechnology* 29 (25): 255303. <https://doi.org/10.1088/1361-6528/aabb79>.

Jiang, Nan. 2016. "Electron Beam Damage in Oxides: A Review." *Reports on Progress in Physics* 79 (1): 016501. <https://doi.org/10.1088/0034-4885/79/1/016501>.

Jiang, Nan, Eva Zarkadoula, Prineha Narang, Artem Maksov, Ivan Kravchenko, Albina Borisevich, Stephen Jesse, and Sergei V. Kalinin. 2017. "Atom-by-Atom Fabrication by Electron Beam via Induced Phase Transformations." *MRS Bulletin* 42 (09): 653–59.

<https://doi.org/10.1557/mrs.2017.183>.

Jones, Lewys, and Peter D. Nellist. 2013. "Identifying and Correcting Scan Noise and Drift in the Scanning Transmission Electron Microscope." In *Microscopy and Microanalysis*.

<https://doi.org/10.1017/S1431927613001402>.

Kalinin, Sergei V., Albina Borisevich, and Stephen Jesse. 2016. "Fire up the Atom Forge." *Nature* 539 (7630): 485–87. <https://doi.org/10.1038/539485a>.

Kalinin, Sergei V., and Stephen J. Pennycook. 2017. "Single-Atom Fabrication with Electron and Ion Beams: From Surfaces and Two-Dimensional Materials toward Three-Dimensional Atom-by-Atom Assembly." *MRS Bulletin* 42 (09): 637–43.

<https://doi.org/10.1557/mrs.2017.186>.

Kovarik, L., A. Stevens, A. Liyu, and N. D. Browning. 2016. "Implementing an Accurate and Rapid Sparse Sampling Approach for Low-Dose Atomic Resolution STEM Imaging." *Applied Physics Letters* 109 (16): 164102. <https://doi.org/10.1063/1.4965720>.

Krivanek, Ondrej L., Matthew F. Chisholm, Valeria Nicolosi, Timothy J. Pennycook, George J. Corbin, Niklas Dellby, Matthew F. Murfitt, et al. 2010. "Atom-by-Atom Structural and Chemical Analysis by Annular Dark-Field Electron Microscopy." *Nature* 464 (7288): 571–74. <https://doi.org/10.1038/nature08879>.

Krivanek, Ondrej L., Tracy C. Lovejoy, Niklas Dellby, Toshihiro Aoki, R. W. Carpenter, Peter Rez, Emmanuel Soignard, et al. 2014. "Vibrational Spectroscopy in the Electron Microscope." *Nature* 514 (7521): 209–12. <https://doi.org/10.1038/nature13870>.

- Mallat, Stephane. 2009. *A Wavelet Tour of Signal Processing. A Wavelet Tour of Signal Processing*. Elsevier/Academic Press. <https://doi.org/10.1016/B978-0-12-374370-1.50001-9>.
- McMullan, G., A.T. Clark, R. Turchetta, and A.R. Faruqi. 2009. "Enhanced Imaging in Low Dose Electron Microscopy Using Electron Counting." *Ultramicroscopy* 109 (12): 1411–16. <https://doi.org/10.1016/J.ULTRAMIC.2009.07.004>.
- McMullan, G., A.R. Faruqi, D. Clare, and R. Henderson. 2014. "Comparison of Optimal Performance at 300keV of Three Direct Electron Detectors for Use in Low Dose Electron Microscopy." *Ultramicroscopy* 147 (December): 156–63. <https://doi.org/10.1016/j.ultramic.2014.08.002>.
- Muller, A., and J. Grazul. 2001. "Optimizing the Environment for Sub-0.2 Nm Scanning Transmission Electron Microscopy." *Journal of Electron Microscopy* 50 (3): 219–26. <https://doi.org/10.1093/jmicro/50.3.219>.
- Okunishi, E, I Ishikawa, H Sawada, F Hosokawa, M Hori, and Y Kondo. 2009. "Visualization of Light Elements at Ultrahigh Resolution by STEM Annular Bright Field Microscopy." *Microscopy and Microanalysis* 15 (S2): 164–65. <https://doi.org/10.1017/S1431927609093891>.
- Paleo, Pierre. 2016. "PDWT:A GPU Implementation of the Wavelet Transform." <https://github.com/pierrepaleo/PDWT>.
- Pennycook, Stephen J. 2017. "The Impact of STEM Aberration Correction on Materials Science."

Ultramicroscopy 180: 22–33. <https://doi.org/10.1016/j.ultramic.2017.03.020>.

Pennycook, Timothy J., Andrew R. Lupini, Hao Yang, Matthew F. Murfitt, Lewys Jones, and Peter D. Nellist. 2015. “Efficient Phase Contrast Imaging in STEM Using a Pixelated Detector. Part 1: Experimental Demonstration at Atomic Resolution.” *Ultramicroscopy* 151 (April): 160–67. <https://doi.org/10.1016/J.ULTRAMIC.2014.09.013>.

Peyré, Gabriel. 2011. “The Numerical Tours of Signal Processing.” *Computing in Science and Engineering* 13 (4): 94–97. <https://doi.org/10.1109/MCSE.2011.71>.

Reed, Bryan W., Sang Tae Park, and Daniel J. Masiel. 2016. “Quantifying the Advantages of Compressive Sensing and Sparse Reconstruction for Scanning Transmission Electron Microscopy.” *Microscopy and Microanalysis* 22 (S3): 286–87. <https://doi.org/10.1017/S1431927616002282>.

Sang, Xiahan, Andrew R. Lupini, Raymond R. Unocic, Miaofang Chi, Albina Y. Borisevich, Sergei V. Kalinin, Eirik Endeve, Richard K. Archibald, and Stephen Jesse. 2017. “Dynamic Scan Control in STEM: Spiral Scans.” *Advanced Structural and Chemical Imaging* 2 (1): 6. <http://ascimaging.springeropen.com/articles/10.1186/s40679-016-0020-3>.

Stevens, A., L. Luzi, H. Yang, L. Kovarik, B. L. Mehdi, A. Liyu, M. E. Gehm, and N. D. Browning. 2018. “A Sub-Sampled Approach to Extremely Low-Dose STEM.” *Applied Physics Letters* 112 (4): 043104. <https://doi.org/10.1063/1.5016192>.

Stevens, Andrew, Hao Yang, Lawrence Carin, Ilke Arslan, and Nigel D. Browning. 2014. “The Potential for Bayesian Compressive Sensing to Significantly Reduce Electron Dose in High-

Resolution STEM Images.” *Microscopy* 63 (1): 41–51.

<https://doi.org/10.1093/jmicro/dft042>.

Susi, Toma, Demie Kepaptsoglou, Yung-Chang Lin, Quentin M Ramasse, Jannik C Meyer, Kazu Suenaga, and Jani Kotakoski. 2017. “Towards Atomically Precise Manipulation of 2D Nanostructures in the Electron Microscope.” *2D Materials* 4 (4): 042004.

<https://doi.org/10.1088/2053-1583/aa878f>.

Susi, Toma, Jani Kotakoski, Demie Kepaptsoglou, Clemens Mangler, Tracy C. Lovejoy, Ondrej L. Krivanek, Recep Zan, et al. 2014. “Silicon–Carbon Bond Inversions Driven by 60-KeV Electrons in Graphene.” *Physical Review Letters* 113 (11): 115501.

<https://doi.org/10.1103/PhysRevLett.113.115501>.

Susi, Toma, Jannik C. Meyer, and Jani Kotakoski. 2017. “Manipulating Low-Dimensional Materials down to the Level of Single Atoms with Electron Irradiation.” *Ultramicroscopy* 180 (September): 163–72. <https://doi.org/10.1016/j.ultramic.2017.03.005>.

Tuma, Tomas, John Lygeros, V Kartik, Abu Sebastian, and Angeliki Pantazi. 2012. “High-Speed Multiresolution Scanning Probe Microscopy Based on Lissajous Scan Trajectories.” *Nanotechnology* 23 (18): 185501. <https://doi.org/10.1088/0957-4484/23/18/185501>.

Tuma, Tomas, John Lygeros, Abu Sebastian, and Angeliki Pantazi. 2013. “Analysis and Design of Multiresolution Scan Trajectories for High-Speed Scanning Probe Microscopy.” In *IFAC Proceedings Volumes (IFAC-PapersOnline)*, 46:138–44. <https://doi.org/10.3182/20130410-3-CN-2034.00052>.

Wang, Zhou, Alan Conrad Bovik, Hamid Rahim Sheikh, and Eero P. Simoncelli. 2004. "Image Quality Assessment: From Error Visibility to Structural Similarity." *IEEE Transactions on Image Processing* 13 (4): 600–612. <https://doi.org/10.1109/TIP.2003.819861>.

Yong, Y K, A Bazaei, S O R Moheimani, and F Allg. 2012. "Design and Control of a Novel Non-Raster Scan Pattern for Fast Scanning Probe Microscopy." *ieeexplore.ieee.Org*, 456–61. <https://ieeexplore.ieee.org/abstract/document/6266062/>.

Zhao, Xiaoxu, Jani Kotakoski, Jannik C. Meyer, Eli Sutter, Peter Sutter, Arkady V. Krasheninnikov, Ute Kaiser, and Wu Zhou. 2017. "Engineering and Modifying Two-Dimensional Materials by Electron Beams." *MRS Bulletin* 42 (09): 667–76. <https://doi.org/10.1557/mrs.2017.184>.

Zhou, Wu, Mark P. Oxley, Andrew R. Lupini, Ondrej L. Krivanek, Stephen J. Pennycook, and Juan-Carlos Idrobo. 2012. "Single Atom Microscopy." *Microscopy and Microanalysis* 18 (06): 1342–54. <https://doi.org/10.1017/S1431927612013335>.

